

# Plasmonic Nano-Rotamers with Programmable Polarization-Resolved Coloration

Juhwan Kim, Jang-Hwan Han, Hyun Min Kim, Tung-Chun Lee,\* and Hyeon-Ho Jeong\*

**3D-shaped artificial Mg nano-rotamers with a programmable dihedral angle between two plasmonic arms, designed to exhibit both programmable linear and circular polarization properties, are presented. The nanoscale physical shadow growth technique offers precise control over the angular alignment in these nanostructures with 1° angular precision, thus controlling their symmetry from achiral  $C_{2v}$  and  $C_{2h}$  to chiral  $C_2$ . As a result, they give rise to a wide range of polarization-resolved coloration, spanning from invisible to visible colors with 46% transmission contrast for linear polarization while exhibiting 0.08  $g$ -factor in visible for circular polarization. These nano-rotamers hold great potential for various applications in adaptive photonic filters, memory, and anticounterfeiting devices, benefiting from their tunable plasmonic properties.**

immense potential for polarization-sensitive optical metamaterials that are currently beyond reach.<sup>[3–9]</sup> Plasmonic isomers, such as dimers<sup>[1]</sup> and trimers,<sup>[10]</sup> arise distinct coupled resonance when illuminated with linearly polarized light along their long axis, offering a wide range of applications in optical devices including, filters,<sup>[11,12]</sup> sensors,<sup>[13,14]</sup> and encryption.<sup>[15,16]</sup> Recent advances in nanofabrication techniques have further facilitated the realization of 3D structural nano-architecture, enabling the exploration of enantiomers, i.e., stereoisomers that are not superimposable with their mirror image.<sup>[17–19]</sup> Chiral helicoids<sup>[20]</sup> and helices,<sup>[21]</sup> for instance, inherently offer strong optical activity, showcasing

differential plasmonic resonance when subjected to circularly polarized light. These properties find utility in molecular sensing<sup>[22]</sup> and holographic imaging devices.<sup>[23–25]</sup>

Expanding along this line, a fascinating molecular group to explore further is that of rotational isomers. Rotamers are molecules composed of two or more parts arranged with a specific dihedral angle, leading to unique polarization-resolved coloration in their plasmonic counterparts.<sup>[26–28]</sup> Rich programming in their associated dihedral angle allows a high degree of tunability in the symmetry ranging from achiral  $C_{2v}$  and  $C_{2h}$  to chiral  $C_2$ , potentially enabling color dynamics for both linearly and circularly polarized light in distinct spectral ranges. Recently, the DNA origami-assisted plasmonic nano-rotamers have been reported, featuring reconfigurable chiroptical responses according to the angular arrangements between the isomers.<sup>[29]</sup> This is a crucial step toward polarization-resolved plasmonic elements, but it is still hindered for large-area device applications by challenges associated with the mass production of nano-rotamers with identical optical dynamics.

Here we demonstrate a wafer-scale “lithography-free” parallel fabrication scheme to realize 3D-shaped Mg nano-rotamers acting as a dual functional plasmonic architecture, allowing us to program both linear and circular polarization-resolved coloration, which is challenging to achieve otherwise. Using a physical shadow growth technique known as glancing angle deposition (GLAD),<sup>[30,31]</sup> we demonstrate controlled precise variations in the dihedral angles of an array of nano-rotamers across from achiral  $C_{2v}$  to various types of chiral  $C_2$  symmetric structures. This engineering flexibility results in wafer-level polarization-resolved coloration for both linearly and circularly polarized lights, spanning

## 1. Introduction


Plasmonic molecules are discreet fundamental building blocks comprising multiple metallic nano-motifs arranged in a specific geometric form, giving rise to intriguing light-matter interactions akin to those observed in molecular systems.<sup>[1,2]</sup> The ability to design plasmonic molecules at the nanoscale holds

J. Kim, J.-H. Han, H. M. Kim, H.-H. Jeong  
School of Electrical Engineering and Computer Science  
Gwangju Institute of Science and Technology  
Cheomdangwagi-ro 123, Gwangju 61005, Republic of Korea  
E-mail: jeong323@gist.ac.kr

T.-C. Lee  
Institute for Materials Discovery  
University College London  
London WC1H 0AJ, UK  
E-mail: tungchun.lee@ucl.ac.uk

T.-C. Lee  
Department of Chemistry  
University College London  
London WC1H 0AJ, UK

H.-H. Jeong  
Department of Semiconductor Engineering  
Gwangju Institute of Science and Technology  
Cheomdangwagi-ro 123, Gwangju 61005, Republic of Korea

 The ORCID identification number(s) for the author(s) of this article can be found under <https://doi.org/10.1002/adom.202301730>

© 2023 The Authors. Advanced Optical Materials published by Wiley-VCH GmbH. This is an open access article under the terms of the Creative Commons Attribution License, which permits use, distribution and reproduction in any medium, provided the original work is properly cited.

DOI: 10.1002/adom.202301730

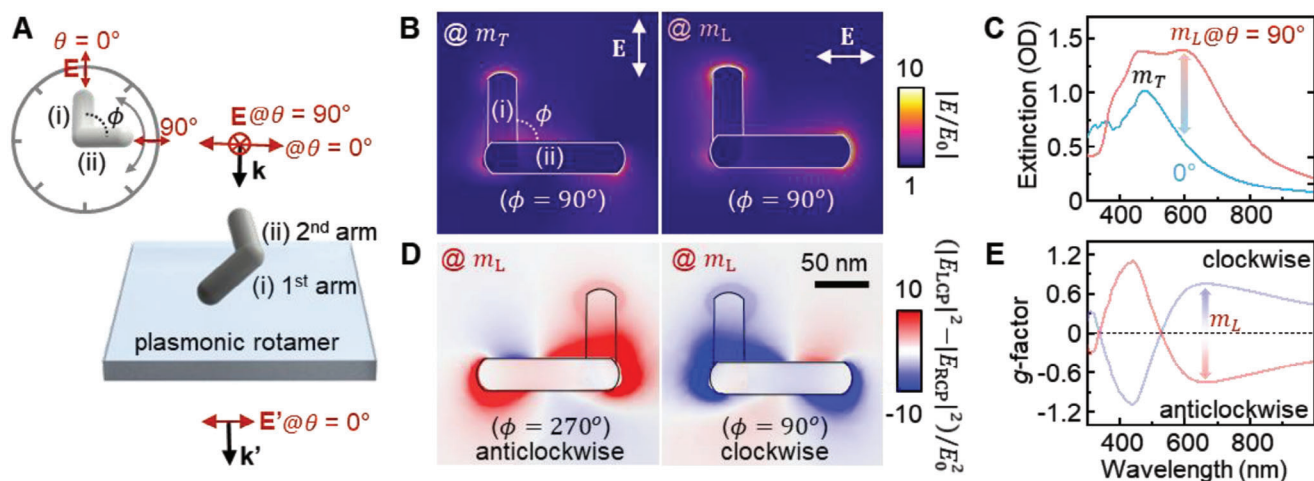


**Figure 1.** Plasmonic nano-rotamers with programmable polarization-resolved resonance. A) Scheme showing a 3D-shaped plasmonic nano-rotamer with a dihedral angle  $\phi = 90^\circ$  under two different linear polarization states ( $\theta = 0^\circ$  and  $90^\circ$ ) of an incident white light, where the light polarized along the second arm (i.e.,  $\theta = 90^\circ$ ) is blocked by the plasmonic nano-rotamer. B) Associated numerical calculation on the optical near-field enhancement of the single nano-rotamer excited by a linearly polarized light at  $\theta = 0^\circ$  to excite transverse mode,  $m_T$  (left), and  $\theta = 90^\circ$  to excite longitudinal mode,  $m_L$  (right). C) Plasmonic extinction spectra of a hexagonal array of the nano-rotamer with 100 nm center-to-center spacing versus the polarization angle  $\theta$  from  $0^\circ$  to  $90^\circ$ . D) Chiral optical near-field enhancements of the anticlockwise (left) and clockwise nano-rotamers (right) under the left and right circularly-polarized lights at resonance E) and the  $g$ -factor of their arrays with 100 nm center-to-center spacing.

from transparent to visible colors, opening up numerous possibilities for a wide range of nanophotonic applications.

## 2. Results and Discussion

### 2.1. Concept of Plasmonic Nano-Rotamers

Drawing inspiration from an analog clock, which utilizes minute and hour arms to present a wide array of rotational configurations, we here present 3D-shaped nano-rotamers with controllable dihedral angle  $\phi$  between two arms, exhibiting polarization-resolved plasmonic resonance, **Figure 1A**. Strictly speaking, these plasmonic nano-rotamers are geometrically continuous and static, which clearly differ from those seen in their molecular counterparts.<sup>[32,33]</sup> However, their polarization-dependent plasmonic behaviors hypothetically mimic the optical characteristics of the molecular rotamers, so we believe they are still valid as “plasmonically” acting rotamers.

Similar to the plasmonic characteristics of Au nanorods, which exhibit distinctive transverse (short axis,  $m_T$ ) and longitudinal (long axis,  $m_L$ ) resonance modes,<sup>[34]</sup> a 3D-shaped nano-rotamer, for instance, with a dihedral angle of  $\phi = 90^\circ$  (i.e.,  $C_2$  symmetry) also displays two dominant features depending on the excited resonance modes, leading to different extinction spectra. Notably, we employ Mg as the base material for these nano-rotamers, as it offers plasmonic resonances in the ultraviolet spectral window for small structures (i.e., invisible),<sup>[35]</sup> which red-shifts into the visible regime as the length increases, analogous to the tuning in resonance from the aspect ratio of the rod (Figure S1, Supporting Information). For example, the nano-rotamer with a dihedral angle of  $\phi = 90^\circ$  reveals a distinct color supported by the plasmonic extinction (i.e., the sum of scattering and absorption) when linearly polarized light is irradiated along its long axis of the second arm. This condition satisfies  $\theta = \phi$ , which we term

$m_L$  mode. Here, we assign  $\theta = 0^\circ$  for the linearly polarized light aligned with the long axis of the first arm of the rotamer. Conversely, when linearly polarized light aligns with the short axis of the second arm of the rotamer, it excites UV plasmonic resonance, a condition we term  $m_T$  mode ( $\theta \perp \phi$ ), **Figure 1A**. Numerical simulations using the finite element method (FEM) suggest that by rotating the linear polarization angle to match the orientation of the nano-rotamer, differences in optical near-field enhancements emerge (**Figure 1B**), leading to variations in far-field extinction spectra (**Figure 1C**). As an example, we consider the rotamer with  $\phi = 90^\circ$  designed with each arm’s dimensions of 120 nm length and 30 nm width, values obtained from the fabricated samples below. The projection images of the optical near-field enhancements in air presented in **Figure 1B** combine data from two representative 2D optical field distributions along the long axes of the first and second arms of the rotamer (**Figure S2**, Supporting Information). These images reveal variations in the optical near-field enhancements, particularly at the edges of the long axis of the second arm of the rotamer between  $\theta = \phi$  and  $\theta \perp \phi$  orientations. This discrepancy causes a notable color change with a 40% switching contrast at the  $m_L$  resonance for the rotamers arranged with a center-to-center spacing of 100 nm (**Figure 1C**, see also **Figure S3**, Supporting Information for the simulated spectra of single nano-rotamer). This is because Mg nanostructures offer resonances in UV, which remains invisible to the naked eye, while still retaining plasmonic activity ( $m_T$ ) when  $\theta \perp \phi$ . This property promises a switchable color appearance, transiting from invisible to vibrant colors with high spatial definition. Furthermore, the slanted structural profile of this plasmonic nano-rotamer inherently holds geometrical  $C_2$  chirality, thus inducing discrete optical near-field enhancements when subjected to the left and right circularly polarized lights (**Figure 1D**). This enhancement can be further engineered with the dihedral angle  $\phi$  and gives rise to tunable differential extinction spectra and thus unique

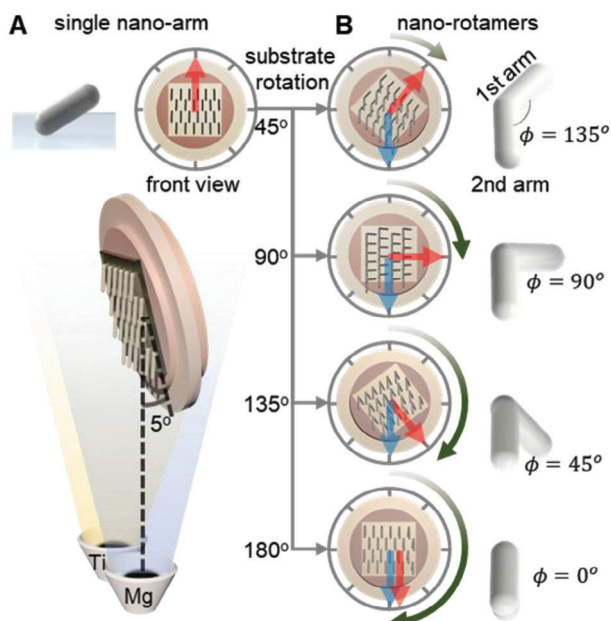


**Figure 2.** Glancing angle deposition (GLAD) for the fabrication of A) single nano-arms and B) nano-rotamers with different substrate angles.

chiroptical signatures, Figure 1E. We experimentally confirm these phenomena using wafer-scale plasmonic nano-rotamers.

## 2.2. Wafer-Scale Array of Plasmonic Nano-Rotamers

The large-scale parallel growth of Mg nano-rotamers using GLAD allows precise control over the size, shape, and material composition of the nanoparticles.<sup>[21,36]</sup> There are prior similar approaches, i.e., using GLAD-grown structures for modulating the light polarization.<sup>[37,38]</sup> They are based on a “seed-free” conventional GLAD approach to grow irregular dielectric nanostructures with a structural resolution of several hundred nanometers. These nanostructures are able to modulate the speed (i.e., phase) and intensity of light when propagating through them. Meanwhile, to make the nanostructures plasmonically active, they need to be formed with metallic materials with dimensions below 100 nm, which are extremely difficult to achieve using the conventional GLAD alone. We thus introduce the nanoscale seeds to first pattern a substrate with a quasi-hexagonal array of 10 nm Au nanodots using block-copolymer micelle nanolithography (BCML), Figure S4 (Supporting Information).<sup>[39]</sup> After that, the GLAD technique is used to selectively grow slanted Mg nano-arms onto each Au nanodot through a self-shadowing effect with the substrate angle nearly parallel to molecular vapor flux (Figure 2).<sup>[40]</sup> During the growth process, due to the fast diffusion of the Mg adatoms, we introduce 5% titanium (Ti) doping, which enhances the structural shaping in 3D while preserving the strong plasmonic property.<sup>[22,41]</sup> The long axis of the arms is readily controllable within the range of 50–200 nm, as determined through analysis of the scanning electron microscopic (SEM) images versus the measured thickness using the quartz crystal microbalance (QCM) monitor during growth (Figure S5, Supporting Information). Here, to enable systematic structural engineering

while emphasizing the key feature of nano-rotamers, we fix the length of the plasmonic arms to 120 nm (Figure 2A) and create nano-rotamers with varying the dihedral angle  $\phi$  by simply rotating the azimuthal angle of the substrate matching to  $\phi$  and growing identical slanted 2nd Mg arms on top (Figure 2B; see also Figures S6–S8, Supporting Information for SEM images). In contrast to their classical molecular analogs, e.g., *n*-butane and H<sub>2</sub>O<sub>2</sub> at room temperature,<sup>[42,43]</sup> these GLAD-grown nano-rotamers are structurally static at room temperature due to the high rotational kinetic barrier at the connection between the two arms compared to thermal energy, and thus cannot interconvert. They nevertheless exhibit much stronger polarization-resolved coloration compared to the angular polarizability of molecular rotamers, which is indeed beneficial for device application.

The optical characteristics of the GLAD-grown plasmonic single nano-arms and nano-rotamers (double arms with a dihedral angle) are examined and imaged under a white light source with a linear polarizer (polarization angular rotation from 0° to 180° with 5° intervals), Figure 3. Note that special protections are necessary when using the Mg rotamers in a solution-based environment,<sup>[35,40]</sup> but the presence of a native oxide layer around the Mg rotamers renders them stable in ambient air, which is the measurement condition here.<sup>[44]</sup> So, a monolayer of single Mg plasmonic arms with a length of 120 nm and a width of 30–40 nm is measured in air (Figure 3A,B) and gives rise to the plasmonic extinction of  $\approx 0.2$  optical density, OD (63% decay in transmittance) at  $m_1$  in visible (601 nm of wavelength) when linearly polarized light is irradiated along the long axis of the single arm at  $\theta = 0^\circ$ . This plasmonic extinction diminishes completely down to 0.02 OD when the polarization axis turns to  $\theta = 90^\circ$  (i.e., normal to the long axis of the single arms), Figure 3C,D. Crucially the plasmonic nano-rotamers with  $\phi = 0^\circ$  between the first arms (120 nm length) and second arms (120 nm length, Figure 3E) display nearly identical spectral features but exhibit twice larger switching contrast compared to the single arms, Figure 3F,G. This enhancement in the contrast arises from the fact that the number of plasmonic resonators is double in the optical path, i.e., twice larger in length (Figure S9, Supporting Information), suggesting that even larger switching contrast can be achieved by increasing the number of arms viz. zigzag structures. Note that, due to inherent challenges involved in parallel growth at the nanoscale, including i) imperfections in the array of Au nanodots for the GLAD process, ii) fluctuations in the deposition rate due to the low melting temperature of Mg, and iii) high diffusion of Mg adatoms on the surface, there is a considerable variation in size and shape among the nano-rotamers, leading to broadened harmonic resonance spectra. Nonetheless, such broad resonance spectra across the whole visible range by averaging optical responses of a large number of nano-rotamers within the beam spot area of 0.8 cm<sup>2</sup> indeed hold potential for various photonic device applications including photodetectors and photovoltaics.<sup>[45–47]</sup> More crucially, these spectra still function to fully switch off through the whole visible spectra at  $\theta = 90^\circ$ . We, therefore, observe almost identical optical dynamics under the same polarization conditions for both single nano-arms and nano-rotamers across the entire visible spectra (Figure 3H), establishing a crucial basis for exploring various types of nano-rotamers with dihedral angular engineering.



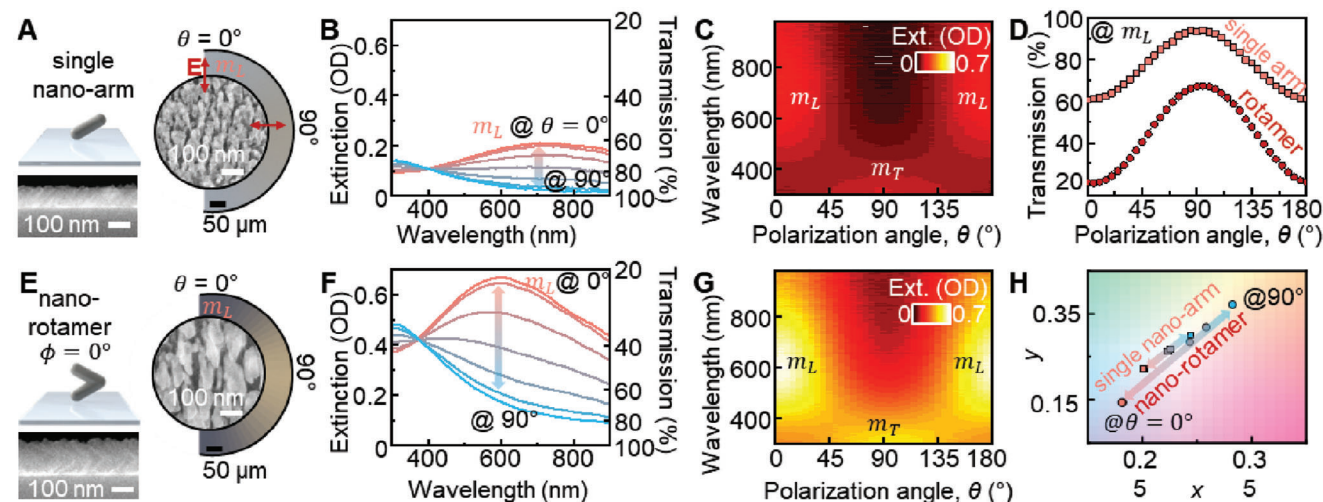


**Figure 3.** Plasmonic single nano-arms and nano-rotamers with double arms for  $C_{2v}$  symmetry. A) An array of plasmonic single nano-arms (half-circular inset: a series of transmitted optical images with every  $5^\circ$  polarization angle changes) and B) their extinction and transmission spectra, C) linear polarization-resolved extinction in the 2D map, and D) peak intensities versus the polarization angle,  $\theta$  ranging from  $0^\circ$  to  $180^\circ$ . E) An array of plasmonic nano-rotamers with a dihedral angle,  $\phi = 0^\circ$  (half-circular inset: a series of transmitted optical images with every  $5^\circ$  polarization angle changes) and F) their extinction and transmission spectra, G) linear polarization-resolved extinction in 2D map versus the polarization angle,  $\theta$ . H) 1913 CIE plot of the transmitted colors through the plasmonic single nano-arms and nano-rotamers with  $\phi = 0^\circ$ .

### 2.3. Plasmonic Nano-Rotamers with Angular Rotation Engineering

To investigate how this nano-rotamer's optical dynamics are sensitive to structural parameters, we fabricate a series of the plasmonic nano-rotamers with various dihedral angles  $\phi = 45^\circ$ ,  $90^\circ$ ,  $135^\circ$ ,  $-135^\circ$  (Figure 4), verified through SEM imaging (Figure 4A; Figures S6–S8, Supporting Information). Since these plasmonic nano-rotamers possess  $C_2$  chiral symmetry, they thus differently interact with linearly as well as circularly polarized lights. First, we analyze their optical dynamics in response to the linearly polarized white light with the angular rotation from  $0^\circ$  to  $180^\circ$  with  $5^\circ$  intervals, Figure 4B. The spectral tuning of the nano-rotamers as a function of the dihedral angle  $\phi$  is characterized experimentally and compared to simulation results, revealing a characteristic reversible 30% switching contrast (Figure 4C). Notably, almost identical color spectra across the whole visible range arise when the light polarization is aligned with every two long axes of the rotamers unless otherwise remaining centered around in the CIE plot indicating invisible (Figure 4D). These excellent dynamic optical performances, coupled with high fidelity in angular engineering, are found to be in reasonable agreement with the predictions of the numerical simulation (Figure S10, Supporting Information). Furthermore, the polarization-resolved colorations, featuring a transition from color to transparency, present larger wavelength switching with relatively high contrasts, compared to previous devices (Figure S11A, Supporting Information), offering exciting opportunities for modulating light transmission in various photonic applications including adaptive color filters,<sup>[27,48,49]</sup> optical memory and security devices,<sup>[50,51]</sup> and covert display.<sup>[38]</sup>

We stress that thanks to the slanted structural profiles of these plasmonic nano-rotamers with intrinsic geometrical  $C_2$  chirality, strong chiroptical responses with significant spectral switch-

ing are possible in the visible range when illuminated with circularly polarized white lights, Figure 5. The circular dichroism (CD) spectra provide a means to identify the chiroptical properties of the plasmonic nano-rotamers by differentiating their extinction in response to the left and right circularly polarized lights, Figure 5A. Remarkably, the plasmonic nano-rotamers with clockwise rotation angles of  $\phi = 0^\circ$ ,  $45^\circ$ ,  $90^\circ$ , and  $135^\circ$  exhibit consistent polar CD spectra with large  $g$ -factor tuning from  $\approx 0$  to 0.08 which can be reversed when the rotation is anticlockwise (Figure 5B,C).<sup>[29]</sup> While the formation of nanostructures on the glass surface often introduces extrinsic chiroptical effects,<sup>[52]</sup> we successfully confirm the intrinsic chiroptical characteristics of the nano-rotamers from their identical spectra irrespective of the incident light direction, as they are truly chiral in 3D (Figure S12, Supporting Information). These experimental findings are in agreement with the numerically simulated spectra, where the associated chiroptical near-field enhancements vary with the rotational angle, thus causing the observed tuning of the CD spectra (Figure 5C). The significant disparities in  $g$ -factors between the simulations and the experiments primarily arise from constraints related to the fabrication process, essentially involving large structural variations in length, width, and angle of the arms of the rotamers as well as their arrangements. Consequently, the experimentally broad extinction spectra occur in response to the circularly polarized lights (Figure S13, Supporting Information), resulting in low  $g$ -factors. This effect is particularly pronounced for the nano-rotamer with  $\phi = 90^\circ$ , as their certain angles intrinsically possess achiral features, analogous to L-shaped structures.<sup>[19]</sup> Nevertheless, the nano-rotamers still present high  $g$ -factors at relatively shorter wavelengths compared to those observed in previous chiral plasmonic nanostructures (Figure S11B, Supporting Information). We thus believe that such fine tunability in the chiroptical response of the plasmonic nano-rotamers holds great promise for chirality-driven

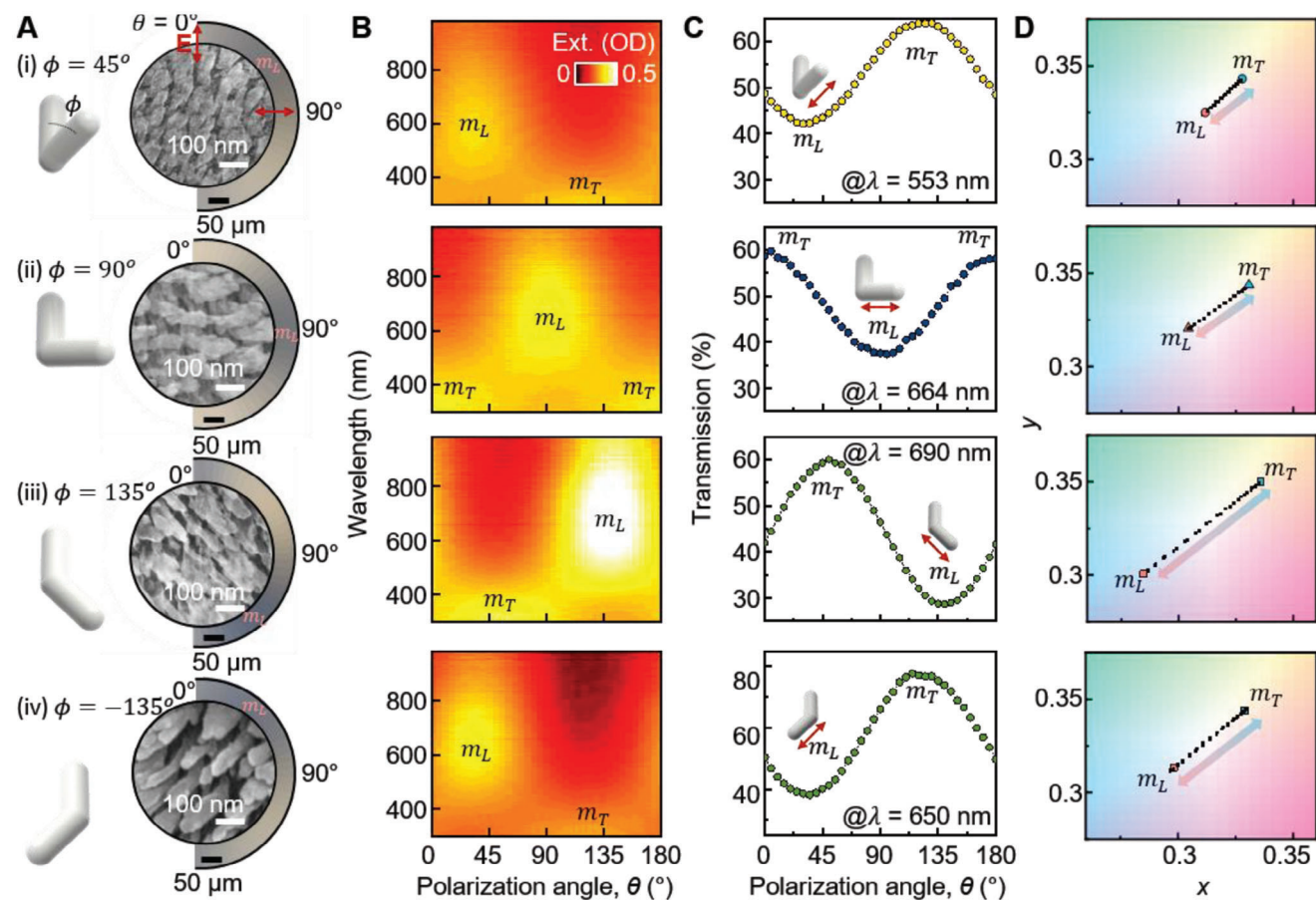


**Figure 4.** Plasmonic nano-rotamers with varying dihedral angles. A) An array of plasmonic nano-rotamers with dihedral angles,  $\phi = 45^\circ, 90^\circ, 135^\circ, -135^\circ$  (from top to bottom, each half-circular inset: their transmitted optical images obtained with every  $5^\circ$  polarization angle changes). B) The rotamers' 2D maps of extinction spectra, C) peak intensities of transmission, and D) CIE plots as a function of the polarization angle,  $\theta$  ranging from  $0^\circ$  to  $180^\circ$ .

photonic applications including chiral sensing<sup>[53-55]</sup> and holographic imaging,<sup>[23]</sup> enantiomeric separation,<sup>[56,57]</sup> and chiral-sensitive photo-synthesis<sup>[58]</sup> and photo-catalysts.<sup>[59,60]</sup> Furthermore, although we here deliberately limit the geometrical and material parameters of the plasmonic nano-rotamers to solely highlight the angular engineering fidelity for extensive switching in both linear and circular light polarizations, exploring further engineering spaces may potentially enable rich polarization-resolved coloration, e.g., engineering the angular rotation of the plasmonic nano-rotamers, repeating the arms with complex arrangements, or introducing the nanogap between arms.

### 3. Conclusion

In conclusion, we successfully demonstrate the clock-inspired design of 3D-shaped artificial nano-rotamers made of Mg and their fabrication and optical characterization at the wafer scale, enabling dual programming in linear and circular polarization-resolved colorations. Through the utilization of a physical shadow growth technique, we achieve precise control over the geometrical angular alignment of the plasmonic nano-rotamers, i.e., dihedral angular engineering. This engineering fidelity leads to polarization-resolved reversible coloration switching from in-

visible to visible colors with 50% contrast for linear polarization while giving rise to 0.08 g-factor for circular polarization. Such unique optical properties of these plasmonic nano-rotamers, combined with their "lithography-free" parallel fabrication scheme allow for scalability and large-scale production, paving the way for practical implementation in various polarization-resolved photonic device applications.

### 4. Experimental Section

**Numerical Simulation:** The finite element method using commercial software (COMSOL wave optics module) was used to simulate the optical response of the Mg plasmonic structures on the quartz substrate, assumed to be constant  $n = 1.45$  for calculation simplicity. The nano-arms have a tilt angle of  $40^\circ$  from the plane due to the nature of the GLAD process.<sup>[61]</sup> When calculating the hexagonal array of the nano-rotamers, periodic boundary conditions with the Floquet periodicity were infinitely set along  $x$ - and  $y$ -axes with 100 nm center-to-center spacing. Meanwhile, the perfectly matched layer was formed on both sides of the  $z$ -axis. Optical properties of Mg were taken from the literature,<sup>[62]</sup> and assume that the nano-rotamers were made of pure Mg for calculation simplicity (although the Mg is alloyed with 5% Ti that slightly changes the plasmonic spectral feature).<sup>[63]</sup>

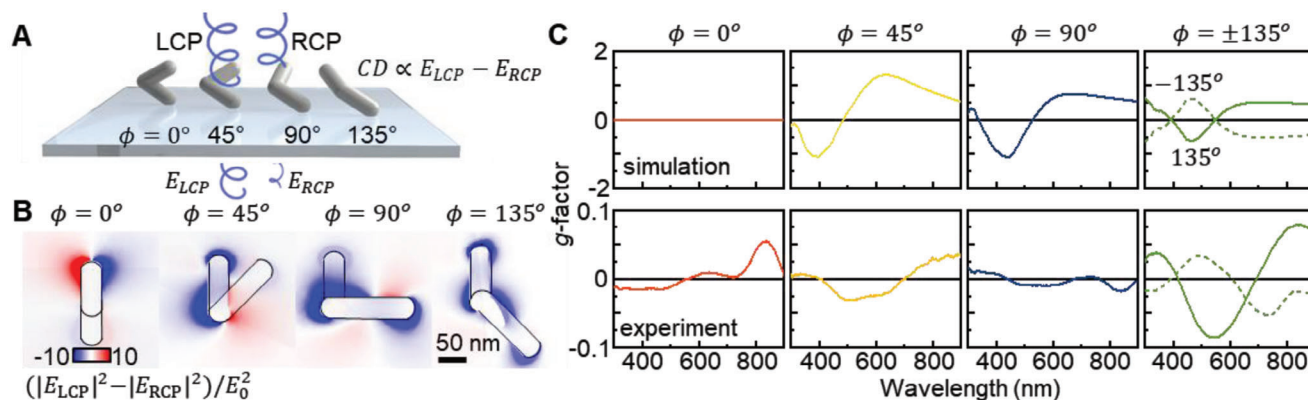


**Figure 5.** Plasmonic nano-rotamers with chiroptical response. A) Scheme showing a plasmonic nano-rotamers under two different circular polarization states of an incident white light. B) Chiroptical near-field enhancement of the nano-rotamers with dihedral angles,  $\phi = 0^\circ, 45^\circ, 90^\circ, \pm 135^\circ$ . C) Numerically calculated (top panel) and experimentally measured (bottom panel) plasmonic extinction spectra of the array of the nano-rotamers.

**Block Copolymer Micelle Nanolithography:** 10 nm Au nanodots were patterned on the substrate using block copolymer micelle nanolithography (BCML) as previously reported.<sup>[39]</sup> The block-copolymer micelles of poly(styrene)-*b*-poly(2-vinyl pyridine) self-assemble in toluene, encapsulating Au salts in their cores. These micelles are then spin-coated onto the 2-inch silicon wafer (for imaging analysis) and quartz substrate (for optical measurement), resulting in a quasi-hexagonal ordered monolayer with a spacing of  $\approx 100$  nm. To remove the polymers and reduce the Au salts, the sample was subjected to a 9:1 gas mixture of an Ar and an O<sub>2</sub> plasma process (100 W, 140 min,  $5 \times 10^{-3}$  torr). This transforms the micelles into Au nanodots with an average diameter of 10 nm, acting as seeds for subsequent GLAD growth.

**Glancing Angle Deposition:** GLAD was used to selectively grow slanted Mg nano-arms onto each Au nanodot through a self-shadowing effect. The growth was carried out at an angle of  $\alpha = 85^\circ$  and temperature of  $\approx 238$  K in a vacuum chamber with a base pressure of  $4 \times 10^{-6}$  Torr. During the growth, Mg and Ti are co-deposited with rates of  $0.1 \text{ nm}^{-1} \text{ s}$  for Mg and  $0.004 \text{ nm}^{-1} \text{ s}$  for Ti. After the growth of Mg single nano-arms, the second growth of the nano-arms is carried out after azimuthally rotating the sample holder to the desired dihedral angle, including  $\phi = 0^\circ, 45^\circ, 90^\circ$ , and  $\pm 135^\circ$ .

**SEM Analysis:** SEM images of the Mg nano-arms and rotamers were obtained using a Verios 5 UC SEM (Thermo Fisher Scientific) at an accelerating voltage of 10 kV. The SEM images of the arrays of BCML seeds, single nano-arms, and nano-rotamers were used to confirm their orderings through the FFT analysis using the Image-J software (Figure S8, Supporting Information).

**Optical Characterization:** Transmitted color images of fabricated samples were taken with a CCD camera (STC-MCS500U3V, Sentech) through  $20\times$  objective (Olympus MPLFLN-BD) in an inverted optical microscope (Olympus GX53) integrated with a linear polarizer (Broadband Polarizer, Edmund Optics) covering a wavelength range from 300 to 2700 nm (polarization angular rotation from  $0^\circ$  to  $180^\circ$  with  $5^\circ$  intervals). The optical extinction spectra were measured with a fiber-optic spectroscopic system (DH-mini deuterium halogen light source, QE Pro spectrometer, Ocean Optics) with the same linear polarizer. A quarter waveplate (Achromatic waveplate, Edmund Optics) is additionally inserted in the optical path after the linear polarizer to generate left and right circularly polarized light for measurement of chiroptical properties.

## Supporting Information

Supporting Information is available from the Wiley Online Library or from the author.

## Acknowledgements

J.K. and J.-H.H. contributed equally. The authors are grateful to the NanoSystems Laboratory at GIST for technical support. The authors also thank to the GIST Central Research Facilities (GCRF) for technical assistance with the SEM imaging and the GIST Nanoinfra for Compound Semiconductors (G-NICS) for access to the cleanroom. This work is supported by the National Research Foundation of Korea (NRF) grant funded by the Korea government (MSIT) (Grant No. NRF-2021R1C1C1005060, NRF-2021M3H3A1037899) and the “regional innovation mega project” program through the Korea Innovation Foundation (2023-DD-UP-0015) funded by Ministry of Science and ICT. J.-H.H. acknowledges support from the AI-based GIST Research Scientist Project.

## Conflict of Interest

The authors declare no conflict of interest.

## Data Availability Statement

The data that support the findings of this study are available from the corresponding author upon reasonable request.

## Keywords

metamolecules, physical shadow growth, plasmonic rotamer, polarization-resolved coloration

Received: July 19, 2023

Revised: October 26, 2023

Published online:

- [1] H.-H. Jeong, M. C. Adams, J.-P. Günther, M. Alarcón-Corraea, I. Kim, E. Choi, C. Mijsch, A. F. Mark, A. G. Mark, P. Fischer, *ACS Nano* **2019**, *13*, 11453.
- [2] C. Jung, S.-J. Kim, J. Jang, J. H. Ko, D. Kim, B. Ko, Y. M. Song, S.-H. Hong, J. Rho, *Sci. Adv.* **2023**, *8*, eabm8598.
- [3] G. Haran, L. Chuntunov, *Chem. Rev.* **2018**, *118*, 5539.
- [4] N. Zohar, L. Chuntunov, G. Haran, *J. Photochem. Photobiol. C Photochem. Rev.* **2014**, *21*, 26.



- [5] R. E. Armstrong, M. Horáček, P. Zijlstra, *Small* **2020**, *16*, 2003934.
- [6] A. N. Koya, *Adv. Photonics Res.* **2022**, *3*, 2100325.
- [7] J.-H. Han, D. Kim, J. Kim, G. Kim, J. T. Kim, H.-H. Jeong, *Nanophotonics* **2022**, *11*, 1863.
- [8] T. Badloe, J. Kim, I. Kim, W.-S. Kim, W. S. Kim, Y.-K. Kim, J. Rho, *Light Sci. Appl.* **2022**, *11*, 118.
- [9] Y. Yang, J. Seong, M. Choi, J. Park, G. Kim, H. Kim, J. Jeong, C. Jung, J. Kim, G. Jeon, K.-I. Lee, D. H. Yoon, J. Rho, *Light Sci. Appl.* **2023**, *12*, 152.
- [10] G. Davison, T. Jones, J. Liu, J. Kim, Y. Yin, D. Kim, W.-I. K. Chio, I. P. Parkin, H.-H. Jeong, T.-C. Lee, *Adv. Mater. Technol.* **2023**, *8*, 2201400.
- [11] T. Shegai, S. Chen, V. D. Miljkovic, G. Zengin, P. Johansson, M. Käll, *Nat. Commun.* **2011**, *2*, 481.
- [12] T. Ellenbogen, K. Seo, K. B. Crozier, *Nano Lett.* **2012**, *12*, 1026.
- [13] L. Chuntonov, G. Haran, *Nano Lett.* **2013**, *13*, 1285.
- [14] D. Punj, R. Regmi, A. Devilez, R. Plauchu, S. B. Moparthi, B. Stout, N. Bonod, H. Rigneault, J. Wenger, *ACS Photonics* **2015**, *2*, 1099.
- [15] P. Zheng, Q. Dai, Z. Li, Z. Ye, J. Xiong, H.-C. Liu, G. Zheng, S. Zhang, *Sci. Adv.* **2021**, *7*, eabg0363.
- [16] M. Song, D. Wang, Z. A. Kudyshev, Y. Xuan, Z. Wang, A. Boltasseva, V. M. Shalaev, A. V. Kildishev, *Laser Photon. Rev.* **2021**, *15*, 2000343.
- [17] M. Hentschel, M. Schäferling, X. Duan, H. Giessen, N. Liu, *Sci. Adv.* **2017**, *3*, e1602735.
- [18] J. T. Collins, C. Kuppe, D. C. Hooper, C. Sibilina, M. Centini, V. K. Valev, *Adv. Opt. Mater.* **2017**, *5*, 1700182.
- [19] E. S. A. Goerlitzer, A. S. Puri, J. J. Moses, L. V. Poulikakos, N. Vogel, *Adv. Opt. Mater.* **2021**, *9*, 2100378.
- [20] H.-E. Lee, H.-Y. Ahn, J. Mun, Y. Y. Lee, M. Kim, N. H. Cho, K. Chang, W. S. Kim, J. Rho, K. T. Nam, *Nature* **2018**, *556*, 360.
- [21] A. G. Mark, J. G. Gibbs, T.-C. Lee, P. Fischer, *Nat. Mater.* **2013**, *12*, 802.
- [22] H.-H. Jeong, A. G. Mark, M. Alarcón-Correa, I. Kim, P. Oswald, T.-C. Lee, P. Fischer, *Nat. Commun.* **2016**, *7*, 11331.
- [23] M. Khorasaninejad, A. Ambrosio, P. Kanhaiya, F. Capasso, *Sci. Adv.* **2016**, *2*, e1501258.
- [24] C. Jung, G. Kim, M. Jeong, J. Jang, Z. Dong, T. Badloe, J. K. W. Yang, J. Rho, *Chem. Rev.* **2021**, *121*, 13013.
- [25] I. Kim, J. Jang, G. Kim, J. Lee, T. Badloe, J. Mun, J. Rho, *Nat. Commun.* **2021**, *12*, 3614.
- [26] M. Sharma, N. Hendler, T. Ellenbogen, *Adv. Opt. Mater.* **2020**, *8*, 1901182.
- [27] E. Heydari, J. R. Sperling, S. L. Neale, A. W. Clark, *Adv. Funct. Mater.* **2017**, *27*, 1701866.
- [28] Z. Li, A. W. Clark, J. M. Cooper, *ACS Nano* **2016**, *10*, 492.
- [29] L. Xin, C. Zhou, X. Duan, N. Liu, *Nat. Commun.* **2019**, *10*, 5394.
- [30] J.-H. Han, D. Kim, J. Kim, G. Kim, P. Fischer, H.-H. Jeong, *Adv. Mater.* **2022**, *35*, 2107917.
- [31] K. Robbie, M. J. Brett, A. Lakhtakia, *Nature* **1996**, *384*, 616.
- [32] Y. Zhang, C. Yu, T. Shan, Y. Chen, Y. Wang, M. Xie, T. Li, Z. Yang, H. Zhong, *Cell Rep. Phys. Sci.* **2022**, *3*, 100765.
- [33] M. Sharafi, J. P. Campbell, S. C. Rajappan, N. Dudkina, D. L. Gray, T. J. Woods, J. Li, S. T. Schneebeli, *Angew. Chem., Int. Ed.* **2017**, *56*, 7097.
- [34] Y. Fang, W.-S. Chang, B. Willingham, P. Swanglap, S. Dominguez-Medina, S. Link, *ACS Nano* **2012**, *6*, 7177.
- [35] H.-H. Jeong, A. G. Mark, P. Fischer, *Chem. Commun.* **2016**, *52*, 12179.
- [36] J. G. Gibbs, A. G. Mark, T.-C. Lee, S. Eslami, D. Schamel, P. Fischer, *Nanoscale* **2014**, *6*, 9457.
- [37] S. Larson, H. Luong, C. Song, Y. Zhao, *J. Phys. Chem. C* **2019**, *123*, 5634.
- [38] J. H. Ko, Y. J. Yoo, Y. J. Kim, S.-S. Lee, Y. M. Song, *Adv. Funct. Mater.* **2020**, *30*, 1908592.
- [39] R. Glass, M. M. Ller, J. P. Spatz, *Nanotechnology* **2003**, *14*, 1153.
- [40] H.-H. Jeong, M. Alarcón-Correa, A. G. Mark, K. Son, T.-C. Lee, P. Fischer, *Adv. Sci.* **2017**, *4*, 1700234.
- [41] Y. He, G. Larsen, X. Li, W. Ingram, F. Chen, Y. Zhao, *Adv. Opt. Mater.* **2015**, *3*, 342.
- [42] Y. Mo, *J. Org. Chem.* **2010**, *75*, 2733.
- [43] Y. Mo, *WIREs Comput. Mol. Sci.* **2011**, *1*, 164.
- [44] E. Ringe, *J. Phys. Chem. C* **2020**, *124*, 15665.
- [45] B. Y. Zheng, Y. Wang, P. Nordlander, N. J. Halas, *Adv. Mater.* **2014**, *26*, 6318.
- [46] R. A. Pala, J. White, E. Barnard, J. Liu, M. L. Brongersma, *Adv. Mater.* **2009**, *21*, 3504.
- [47] S. D. Namgung, R. M. Kim, Y.-C. Lim, J. W. Lee, N. H. Cho, H. Kim, J.-S. Huh, H. Rhee, S. Nah, M.-K. Song, J.-Y. Kwon, K. T. Nam, *Nat. Commun.* **2022**, *13*, 5081.
- [48] H. Jia, Q. J. Wu, C. Jiang, H. Wang, L. Q. Wang, J. Z. Jiang, D. X. Zhang, *Appl. Opt.* **2019**, *58*, 704.
- [49] Y. Jung, H. Jung, H. Choi, H. Lee, *Nano Lett.* **2020**, *20*, 6344.
- [50] R. Feng, H. Wang, Y. Cao, Y. Zhang, R. J. H. Ng, Y. S. Tan, F. Sun, C.-W. Qiu, J. K. W. Yang, W. Ding, *Adv. Funct. Mater.* **2022**, *32*, 2108437.
- [51] Y. Chen, X. Yang, J. Gao, *Light Sci. Appl.* **2019**, *8*, 45.
- [52] J. Karst, N. H. Cho, H. Kim, H.-E. Lee, K. T. Nam, H. Giessen, M. Hentschel, *ACS Nano* **2019**, *13*, 8659.
- [53] R. M. Kim, J.-H. Huh, S. Yoo, T. G. Kim, C. Kim, H. Kim, J. H. Han, N. H. Cho, Y.-C. Lim, S. W. Im, E. Im, J. R. Jeong, M. H. Lee, T.-Y. Yoon, H.-Y. Lee, Q.-H. Park, S. Lee, K. T. Nam, *Nature* **2022**, *612*, 470.
- [54] J. T. Collins, K. R. Rusimova, D. C. Hooper, H.-H. Jeong, L. Ohnoutek, F. Pradaux-Caggiano, T. Verbiest, D. R. Carbery, P. Fischer, V. K. Valev, *Phys. Rev. X* **2019**, *9*, 11024.
- [55] L. Ohnoutek, H.-H. Jeong, R. R. Jones, J. Sachs, B. J. Olohan, D.-M. Rasadean, G. D. Pantos, D. L. Andrews, P. Fischer, V. K. Valev, *Laser Photon. Rev.* **2021**, *15*, 2100235.
- [56] Y. Zhao, A. A. E. Saleh, J. A. Dionne, *ACS Photonics* **2016**, *3*, 304.
- [57] J. García-Guirado, M. Svedendahl, J. Puigdollers, R. Quidant, *Nano Lett.* **2018**, *18*, 6279.
- [58] X. Lu, X. Wang, S. Wang, T. Ding, *Nat. Commun.* **2023**, *14*, 1422.
- [59] L. Tan, S.-J. Yu, Y. Jin, J. Li, P.-P. Wang, *Angew. Chem., Int. Ed.* **2022**, *61*, e202112400.
- [60] Y. Negrín-Montecelo, A. Movsesyan, J. Gao, S. Burger, Z. M. Wang, S. Nlate, E. Pouget, R. Oda, M. Comesaña-Hermo, A. O. Govorov, M. A. Correa-Duarte, *J. Am. Chem. Soc.* **2022**, *144*, 1663.
- [61] M. M. Hawkeye, M. J. Brett, *J. Vac. Sci. Technol. A* **2007**, *25*, 1317.
- [62] K. J. Palm, J. B. Murray, T. C. Narayan, J. N. Munday, *ACS Photonics* **2018**, *5*, 4677.
- [63] G. K. Larsen, Y. He, J. Wang, Y. Zhao, *Adv. Opt. Mater.* **2014**, *2*, 245.